Article

Probing Shapes of Bichromophoric Metal–Organic Complexes Using Ion Mobility Mass Spectrometry

Erin Shammel Baker, John E. Bushnell, Stephen R. Wecksler, Mark D. Lim, Manuel J. Manard, Nicholas F. Dupuis, Peter C. Ford, and Michael T. Bowers

J. Am. Chem. Soc., **2005**, 127 (51), 18222-18228• DOI: 10.1021/ja0553699 • Publication Date (Web): 03 December 2005

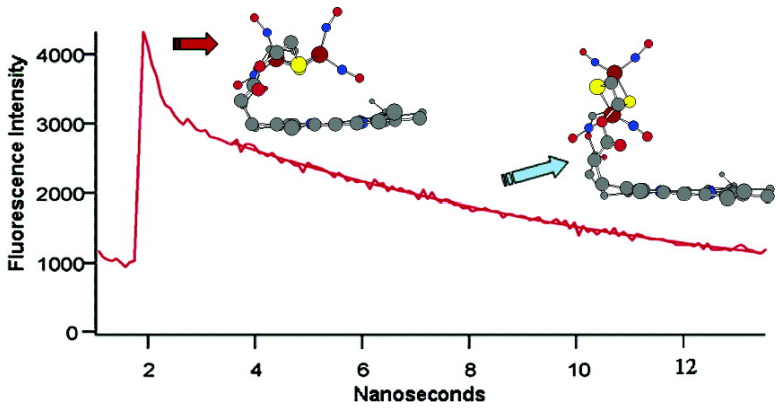

More About This Article

Additional resources and features associated with this article are available within the HTML version:

- Supporting Information
- Links to the 4 articles that cite this article, as of the time of this article download
- Access to high resolution figures
- Links to articles and content related to this article
- Copyright permission to reproduce figures and/or text from this article

View the Full Text HTML

J|A|C|S
ARTICLES
Published on Web 12/03/2005

Probing Shapes of Bichromophoric Metal−Organic Complexes Using Ion Mobility Mass Spectrometry

Erin Shammel Baker, John E. Bushnell, Stephen R. Wecksler, Mark D. Lim, Manuel J. Manard, Nicholas F. Dupuis, Peter C. Ford,* and Michael T. Bowers*

Contribution from the Department of Chemistry and Biochemistry, University of California, Santa Barbara, California 93106-9510

Received August 5, 2005; E-mail: ford@chem.ucsb.edu; bowers@chem.ucsb.edu

Abstract: Ion mobility mass spectrometry (IM-MS) was used to probe the structures of several metal complexes carrying pendant chromophores. The three complexes investigated were the copper(II) complex $Cu(DAC)^{2+}$ (DAC = 1,8-bis(9-methylanthracyl)cyclam, cyclam = 1,4,8,11-tetraazacyclotetradecane), the N-nitrosylated ligand DAC-NO, and the Roussin's red salt ester (μ-*S*,μ-*S*′)-protoporphyrin-IX-bis(2-thioethyl ester)tetranitrosyldiiron (PPIX-RSE). From the IM-MS data coupled with theoretical calculations, it was found that $[Cu^{II}(DAC - H)]^+$ exists as a single conformer, with one anthracenyl group above the cyclam and the other below, similar to the crystal structure of $Cu^{II}(DAC)^{2+}$. The metal-free N-nitrosylated ligand $(DAC\text{-}NO + H)^+$ has two conformations: one family of structures has one anthracenyl group above the cyclam and one below, while the other has both anthracenyl groups on the same side of the cyclam. These observations are consistent with ^{1}H NMR data for the neutral DAC-NO complex that indicate the presence of two geometric isomers in solution. The third species, PPIX-RSE, has a porphyrin chromophore covalently linked to an $Fe_2S_2(NO)_4$ cluster for use as a precursor for the photochemical delivery of nitric oxide in single- and two-photon excitation processes. Ion mobility indicates the presence of two $(PPIX\text{-}RSE + H)^+$ conformations, consistent with the previous interpretation of the bimodal fluorescence lifetime decay seen for PPIX-RSE. DFT structures, in good agreement with the IM-MS cross sections, indicate two "bent" conformations with the planes of the porphyrin and Fe_2S_2 rings at different angles with respect to each other.

Introduction

In recent years, there have been considerable advances in the synthesis of complicated supramolecular species designed to utilize photo-optical properties for applications such as solar energy collection and conversion, molecular machines, photochemical drugs, and fluorescent-based sensors.[1−3] In many cases, these are assembled from several subunits that have their own distinct photochemical and photophysical properties, and in order to understand these properties, the manner by which various subunits may act in concert must be determined. A common type of supramolecular assembly consists of one or more metal complexes linked to well-defined organic chromophores, where the latter serve as antennae to gather light for photochemical reactions and/or as luminescent or absorbing reporters of chemical transformations.[4,5]

Such compounds have been prepared during studies here concerned with exploring photochemical strategies to generate nitric oxide (NO) from metal nitrosyl and nitrito complexes for potential therapeutic purposes[6−13] and with developing sensors for the presence and reactions of small molecules such as

(1) (a) Balzani, V.; Venturi, M, Credi, A. *Molecular Devices and Machines*; Wiley-VCH Verlag GmbH & Co.: Weinheim, Germany, 2003. (b) Balzani, V.; Credi, A.; Raymo, F. M.; Stoddart, J. F. *Angew. Chem., Int. Ed.* **2000**, *39*, 3348.
(2) (a) Miyawaki, A.; Tsien, R. Y. *Methods Enzymol.* **2000**, *327*, 472. (b) Jiang, P.; Guo, Z. *Coord. Chem. Rev.* **2004**, *248*, 205.
(3) (a) Arunkumar, E.; Ajayaghosh, A.; Daub, J. *J. Am. Chem. Soc.* **2005**, *127*, 3156. (b) Tang, W.-S.; Lu, X.-X.; Wong, K. M.-C.; Yam, V. W.-W. *J. Mater. Chem.* **2005**, *15*, 2714.
(4) (a) Straight, S. D.; Andreasson, J.; Kodis, G.; Bandyopadhyay, S.; Mitchell, R. H.; Moore, T. A.; Moore, A. L.; Gust, D. *J. Am. Chem. Soc.* **2005**, *127*, 9403. (b) Haskins-Glusac, K.; Ghiviriga, I.; Abboud, K. A.; Schanze, K. S. *J. Phys. Chem. B* **2004**, *108*, 4969. (c) Hofkens, J.; Cotlet, M.; Vosch, T.; Tinnefeld, P.; Weston, K. D.; Ego, C.; Grimsdale, A.; Muellen, K.; Beljonne, D.; Bredas, J. L.; Jordens, S.; Schweitzer, G.; Sauer, M.; De Schryver, F. *Proc. Natl. Acad. Sci. U.S.A.* **2003**, *100*, 13146. (d) Walters, K. A.; Ley, K. D.; Cavalaheiro, C. S. P.; Miller, S. E.; Gosztola, D.; Wasielewski, M. R.; Bussandri, A. P.; van Willigen, H.; Schanze, K. S. *J. Am. Chem. Soc.* **2001**, *123*, 8329.
(5) (a) Dirksen, A.; Kleverlaan, C. J.; Reek, J. N. H.; De Cola, L. *J. Phys. Chem. A* **2005**, *109*, 5248. (b) Schoonover, J. R.; Dattelbaum, D. M.; Malko, A.; Klimov, V. I.; Meyer, T. J.; Styers-Barnett, D. J.; Gannon, E. Z.; Granger, J. C.; Aldridge, W. S., III; Papanikolas, J. M. *J. Phys. Chem. A* **2005**, *109*, 2472. (c) Feliz, M. R.; Ferraudi, G. *Inorg. Chem.* **2004**, *43*, 1551. (d) Kozlov, D. V.; Castellano, F. N. *Chem. Commun.* **2004**, *24*, 2860. (e) Indelli, M. T.; Ghirotti, M.; Prodi, A.; Chiorboli, C.; Scandola, F.; McClenaghan, N. D.; Puntoriero, F.; Campagna, S. *Inorg. Chem.* **2003**, *42*, 5489. (f) Moore, E. G.; Bernhardt, P. V.; Pigliucci, A.; Riley, M. J.; Vauthey, E. *J. Phys. Chem. A* **2003**, *107*, 8396. (g) Morales, A. F.; Accorsi, G.; Armaroli, N.; Barigelletti, F.; Pope, S. J. A.; Ward, M. D. *Inorg. Chem.* **2002**, *41*, 6711. (h) Argazzi, R.; Bertolasi, E.; Chiorboli, C.; Bignozzi, C. A.; Itokazu, M. K.; Iha, N. Y. M. *Inorg. Chem.* **2001**, *40*, 6885.
(6) (a) Bourassa, J.; DeGraff, W.; Kudo, S.; Wink, D. A.; Mitchell, J. B.; Ford, P. C. *J. Am. Chem. Soc.* **1997**, *119*, 2853. (b) Ford, P. C.; Bourassa, J.; Lee, B.; Lorkovic, I.; Miranda, K.; Laverman, L. *Coord. Chem. Rev.* **1998**, *171*, 185.
(7) (a) Bourassa, J.; Lee, B.; Bernard, S.; Schoonover, J.; Ford, P. C. *Inorg. Chem.* **1999**, *38*, 2947. (b) Bourassa, J. L.; Ford, P. C. *Coord. Chem. Rev.* **2000**, *200−202*, 887.
(8) Lorkovic, I. M.; Miranda, K. M.; Lee, B.; Bernhard, S.; Schoonover, J. R.; Ford, P. C. *J. Am. Chem. Soc.* **1998**, *120*, 11674.
(9) De Leo, M.; Ford, P. C. *J. Am. Chem. Soc.* **1999**, *121*, 1980.
(10) Works, C. F.; Ford, P. C. *J. Am. Chem. Soc.* **2000**, *122*, 7592.

10.1021/ja0553699 CCC: $30.25

NO.[14−16] The photophysics and photochemistry of these materials have been investigated by laser flash photolysis, steady-state fluorescence, fluorescence lifetime measurements, etc. However, determining the three-dimensional structures of chromophore-linked systems that are not conformationally limited represents a major intellectual challenge. Despite the insight that can be gathered by the typical tools to probe structure (X-ray crystallography, NMR, IR, steady-state and dynamic fluorescence, etc.) and by computational techniques, there are limitations in deriving the spatial conformations relevant to in situ molecular dynamics in fluid media. Thus, there is a need for continued development of advanced analytical and computational techniques to overcome such constraints.

Ion mobility mass spectrometry (IM-MS),[17,18] in conjunction with theoretical modeling, is a technique that can be used to evaluate the three-dimensional structure of molecules, since cross sections of theoretical structures can be compared with the experimentally determined cross sections to identify the conformation(s) present in the experiment. IM-MS in conjunction with theoretical calculations has been successfully applied to a variety of compounds, including polymers,[19−21] inorganic cage structures,[22,23] peptides,[24−26] and nucleotides.[27,28]

The focus of the present study is on three compounds (**I**−**III**) with multiple chromophores, shown in Figure 1. The first is the copper(II) complex $Cu(DAC)^{2+}$ (**I**) that has two anthracenyl chromophores linked to the tetradentate ligand cyclam (DAC = 1,8-bis(9-methylanthracyl)cyclam, cyclam = 1,4,8,11-tetraazacyclotetradecane).[14] The anthracenyl groups were attached with the purpose of providing reporters for chemical transformations at the copper center. The interaction of **I** with NO was recently shown to result in formation of the *N*-nitroso cyclam ligand DAC-NO (**II**) (Scheme 1).[14] This unexpected reaction was the first well-characterized example

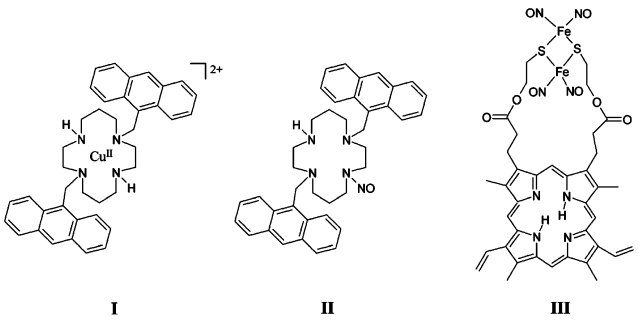

Figure 1. Schematic of $Cu^{II}(DAC)^{2+}$ (**I**), DAC-NO (**II**), and PPIX-RSE (**III**).

Scheme 1. Reaction of **I** with NO

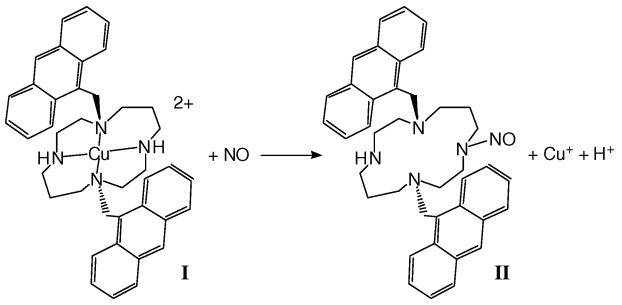

Scheme 2. Possible *E*- and *Z*- Isomers for the Nitrosoamine

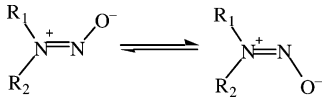

of the reductive nitrosylation of a metal-coordinated ligand. Further analysis using ^{1}H NMR techniques showed that **II** is present as two independent species. Two different types of structures can be proposed, one involving isomerization of the nitrosoamine group with respect to the cyclam ring to give *E*- and a *Z*-isomers (Scheme 2) and the other involving the orientation of the methylanthracenyl groups with respect to the cyclam macrocycle.

The third example, **III**, is an iron−sulfur nitrosyl cluster linked to the protoporphyrin IX chromophore, (*μ*-*S*,*μ*-*S*′)-protoporphyrin-IX-bis(2-thioethyl ester)tetranitrosyldiiron, abbreviated as PPIX-RSE. Roussin's red salt anion $Fe_2S_2(NO)_4^{2-}$ is an effective precursor for photochemical NO release,[6] and the goal in preparing **III** was to attach an antenna (PPIX) that absorbed strongly at longer wavelengths in order to improve the effectiveness of visible-range photolysis.[12] PPIX does indeed serve as an intramolecular sensitizer of the NO labilization from the $Fe_2S_2(NO)_4$ cluster, although quantum yields for NO generation from direct excitation at longer wavelengths (λ_{ex} = 546 nm) were relatively low.[12b] A subsequent study showed that PPIX could also serve as an antenna for two-photon excitation (λ_{ex} = 810 nm) for NO generation from PPIX-RSE.[13] Fluorescence intensity measurements with **III** (intensity about one-sixth that of free PPIX) confirmed that energy transfer from PPIX to the iron cluster was occurring with relatively high efficiency. However, lifetime measurements showed that relaxation from the initial PPIX $\pi-\pi^*$ excited state occurs with two different lifetimes (0.22 and 10.4 ns), both shorter than that of PPIX itself (13.2 ns).[12b] Since this behavior remained even after rigorous repurification, it was concluded that this is

(11) DeRosa, F.; Bu, X.; Ford, P. C. *Inorg. Chem.* **2003**, *42*, 4171.
(12) (a) Conrado, C. L.; Bourassa, J. L.; Egler, C.; Wecksler, S.; Ford, P. C. *Inorg. Chem.* **2003**, *42*, 2288. (b) Conrado, C. L.; Wecksler, S.; Egler, C.; Magde, D.; Ford, P. C. *Inorg. Chem.* **2004**, *43*, 5543.
(13) Wecksler, S.; Mikhailovsky, A.; Ford, P. C. *J. Am. Chem. Soc.* **2004**, *126*, 13566.
(14) Tsuge, K.; DeRosa, F.; Lim, M. D.; Ford, P. C. *J. Am. Chem. Soc.* **2004**, *126*, 6564.
(15) (a) Tran, D.; Ford, P. C. *Inorg. Chem.* **1996**, *35*, 2411. (b) Tran, D.; Skelton, B. W.; White, A. H.; Laverman, L. E.; Ford, P. C. *Inorg. Chem.* **1998**, *37*, 2505.
(16) Ford, P. C.; Lorkovic, I. M. *Chem. Rev.* **2002**, *102*, 993.
(17) (a) Bowers, M. T.; Kemper, P. R.; von Helden, G.; van Koppen, P. A. M. *Science* **1993**, *260*, 1446. (b) von Helden, G.; Hsu, M.-T.; Kemper, P. R.; Bowers, M. T. *J. Chem Phys.* **1991**, *95*, 3835.
(18) Clemmer, D. E.; Jarrold, M. F. *J. Mass Spectrom.* **1997**, *32*, 577.
(19) Gidden, J.; Bowers, M. T.; Jackson, A. T.; Scrivens, J. H. *J. Am. Soc. Mass Spectrom.* **2002**, *13*, 499.
(20) Gidden, J.; Jackson, A. T.; Scrivens, J. H.; Bowers, M. T. *Int. J. Mass Spectrom.* **1999**, *188*, 121.
(21) Gidden, J.; Wyttenbach, T.; Jackson, A. T.; Scrivens, J. H.; Bowers, M. T. *J. Am. Chem. Soc.* **2000**, *122*, 4692.
(22) Gidden, J.; Kemper, P. R.; Shammel, E.; Fee, D. P.; Anderson, S.; Bowers, M. T. *Int. J. Mass Spectrom.* **2003**, *222*, 63.
(23) Baker, E. S.; Gidden, J.; Fee, D. P.; Kemper, P. R.; Anderson, S. E.; Bowers, M. T. *Int. J. Mass Spectrom.* **2003**, *227*, 205.
(24) Wyttenbach, T.; von Helden, G.; Bowers, M. T. *J. Am. Chem. Soc.* **1996**, *118*, 8355.
(25) (a) Bernstein, S. L.; Liu, D.; Wyttenbach, T.; Bowers, M. T.; Lee, J. C.; Gray, H. B.; Winkler, J. R. *J. Am. Soc. Mass Spectrom.* **2004**, *15*, 1435. (b) Bernstein, S. L.; Wyttenbach, T.; Baumketner, A.; Shea, J.-E.; Bitan, G.; Teplow, D. B.; Bowers, M. T. *J. Am. Chem. Soc.* **2005**, *127*, 2075.
(26) (a) Sudha, R.; Kohtani, M.; Breaux, G. A.; Jarrold, M. F. *J. Am. Chem. Soc.* **2004**, *126*, 2777. (b) Kaleta, D. T.; Jarrold, M. F. *J. Am. Chem. Soc.* **2003**, *125*, 7186. (c) Kaleta, D. T.; Jarrold, M. F. *J. Am. Chem. Soc.* **2002**, *124*, 1154.
(27) Gidden, J.; Baker, E. S.; Ferzoco, A.; Bowers, M. T. *Int. J. Mass Spectrom.* **2005**, *240*, 183.
(28) Gidden, J.; Bushnell, J. E.; Bowers, M. T. *J. Am. Chem. Soc.* **2001**, *123*, 5610.

characteristic of PPIX-RSE and likely due to the presence of two different molecular conformations of **III**.

In the present study, IM-MS is applied to the three complexes described above. In the first, the emphasis is on determining whether IM-MS can be used to obtain a structure for **I** and whether this structure is similar to the known crystal structure. Using the results from **I**, the method is then applied to **II** to determine the orientation of the anthracenyl groups relative to the cyclam. Finally, IM-MS is used to find stable structures of **III** and to explore the relationship between these structures and the photophysical dynamics of PPIX-RSE.

Experimental Section

Synthesis and Instrumentation. The syntheses of **I**, **II**, and **III** have been previously reported.[12,14] A custom-built matrix-assisted laser desorption/ionization time-of-flight (MALDI-TOF) instrument was utilized in performing ion mobility experimental analyses on **I**, **II**, and **III**. The details regarding the experimental setup for the mass spectrum and ion mobility measurements have previously been published,[23] so only a brief description will be given here. Ions were formed by MALDI in a home-built ion source with 2,5-dihydroxybenzoic acid (DHB) used as the matrix and methanol (MeOH) as the solvent. Approximately 50 μL of DHB (100 mg/mL), 50 μL of the chromophore sample (1 mg/mL), and 8 μL of NaI (saturated in MeOH) were applied to the sample target and dried. A nitrogen laser ($\lambda = 337$ nm, 12 mW power) was used to generate ions in a two-section (Wiley-McLaren) MALDI-TOF ion source. The ions were accelerated to 9 keV down a 1-m flight tube with the reflectron turned on, in order to obtain high-resolution mass spectra of the ions formed in the source.

To perform ion mobility experiments, the reflectron was turned off, a linear mass gate selected the species of interest, and an opposing voltage was applied to the ions before they entered the drift cell. This caused deceleration of the ions, which prevented collision-induced dissociation and allowed the ions to be gently injected into the 20-cm long glass drift cell filled with ~1.5 Torr of helium gas. The temperature of the cell can be varied from 80 to 500 K, depending on the needs of the experiment. A weak, uniform electric field applied across the cell gently pulled the ions through the He gas at a constant drift velocity. After exiting the drift cell, the ions were gently accelerated through a quadrupole mass filter, which mass selected the ion of interest to be detected. The quadrupole was set to a specific mass-to-charge ratio (m/z) to eliminate any ions that might arise from fragmentation in the drift cell and interfere with the ion mobility experiments. The pulsed source extraction voltage triggered a timing sequence so that the ions were detected as a function of time, yielding an arrival time distribution (ATD). The reduced mobility, K_o, of the ion was accurately determined from a series of ATDs measured at different electric field strengths (7.5−16 V/cm) across the drift cell. Through the use of kinetic theory, the ion's collision cross section was calculated.

Data Analysis. The reduced mobility of the mass selected ions can be obtained using eq 1,[29−30] where l is the length of the cell, T is the temperature in Kelvin, p is the pressure of the He gas (in Torr), V is the strength of the electric field, t_A is the ions' arrival time taken from the center of the ATD peak, and t_o is the amount of time the ion spends outside the drift cell before reaching the detector. A series ATDs are collected by changing the voltage applied to the drift cell. The arrival time (t_A) of each conformer for the ion is determined from the center of each peak in the ATD peak and plotted versus p/V. The t_A vs p/V plot yields a straight line with a slope inversely proportional to K_o and an intercept of t_o. Once K_o is determined, the ion's collision cross section, σ, can be obtained using eq 2, where e is the charge of the ion, N_o is the number density of He at standard temperature and pressure (STP), T is temperature, k_b is Boltzmann's constant, and μ is the ion−He reduced mass.[30]

$$K_o = \left(l^2 \frac{273}{760T} \frac{p}{V} \frac{1}{t_A - t_o} \right) \quad (1)$$

$$\sigma = \frac{3e}{16N_o} \left(\frac{2\pi}{\mu k_b T} \right)^{1/2} \frac{1}{K_o} \quad (2)$$

Theoretical Modeling. To identify the conformers present in the ATDs, theoretical structures were calculated. Two different methods of theoretical modeling were performed, depending on whether the molecule had a transition metal or not. AMBER 7[31] was used to generate the lowest energy theoretical structures for molecules without transition metals, such as $(\mathbf{II} + H)^+$, while density functional theory (DFT) calculations were carried out to generate optimized structures for $(\mathbf{I} - H)^+$ and **III**. AMBER is the preferred method of generating theoretical structures for chromophore-bound complexes because of its ability to quickly generate many structures from one starting structure, whereas DFT takes a long time to perform a geometry optimization on one structure. However, AMBER is not parametrized for transition metals, so DFT calculations are necessary for any chromophore-bound complex with a transition metal.

Using AMBER, trial structures were calculated for $(\mathbf{II} + H)^+$. The proton was located on either of the tertiary nitrogen atoms in the cyclam ring (i.e., those with anthracenyl groups attached). Similar results were obtained in both cases. An annealing/energy minimization cycle was used to generate 200 low-energy structures. In this cycle, an initial minimization of the structure is followed by 30 ps of molecular dynamics at 800 K and 30 ps of molecular dynamics in which the temperature is incrementally dropped to 50 K. The resulting structure is then energy minimized again and used as the starting structure for the next minimization/dynamics run. After the low-energy structures are obtained, theoretical cross sections must be calculated for comparison with experimental cross sections. A temperature-dependent projection model,[32,33] with appropriate atomic collision radii calculated from the ion−He interaction potential, is used to calculate the angle-averaged collision cross section of each theoretical structure. A scatter plot of cross section vs energy is then collected for the minimized structures and used to help identify the ions observed in the experimental ATDs. The average cross section of the lowest 3−5 kcal/mol structures is used for comparison with the experimental cross section.

DFT calculations (B3LYP/LACVP)[34−36] were carried out with the Jaguar program[37,38] to generate optimized structures for $(\mathbf{I} - H)^+$. Multiple chromophore and metal positions were geometry optimized. The cross section was then calculated for the lowest energy theoretical structures with the temperature-dependent projection model described above. The theoretical cross sections obtained for the DFT optimized structures were then compared to the experimentally measured cross sections, in order to determine which theoretical structures correspond to the peaks in the experimental ATDs.

In calculations on **III**, the porphyrin ring is constrained to be nearly planar, and the ion salt is assumed to maintain a structure similar to that of Roussin's red salt, with tetrahedral irons, each bound to two sulfurs and two NO ligands. This leaves the ester linkages between

(29) Maiti, N. C.; Mazumdar, S.; Periaswamy, N. *J. Phys. Chem.* **1995**, *99*, 10708.
(30) Mason, E. A.; McDaniel, E. W. *Transport Properties of Ions in Gases*; Wiley: New York, 1998.
(31) Case, D. A.; et al. *AMBER 7*; University of California: San Francisco, 2002.
(32) von Helden, G.; Hsu, M. T.; Gotts, N.; Bowers, M. T. *J. Phys. Chem.* **1993**, *97*, 8182.
(33) Wyttenbach, T.; von Helden, G.; Batka, J. J., Jr.; Carlat, D.; Bowers, M. T. *J. Am. Soc. Mass Spectrom.* **1997**, *8*, 275.
(34) Stephens, P. J.; Devlin, F. J.; Chabalowski, C. F.; Frisch, M. J. *J. Phys. Chem.* **1994**, *98*, 11623.
(35) Becke, A. D. *J. Chem. Phys.* **1993**, *98*, 5648.
(36) Becke, A. D. *Phys. Rev. A* **1988**, *38*, 3098.
(37) *Jaguar 5.0*; Schrodinger, LLC: Portland, OR, 1991−2003.
(38) Vacek, G.; Perry, J. K.; Langlois, J. M. *Chem. Phys. Lett.* **1999**, *310*, 189.

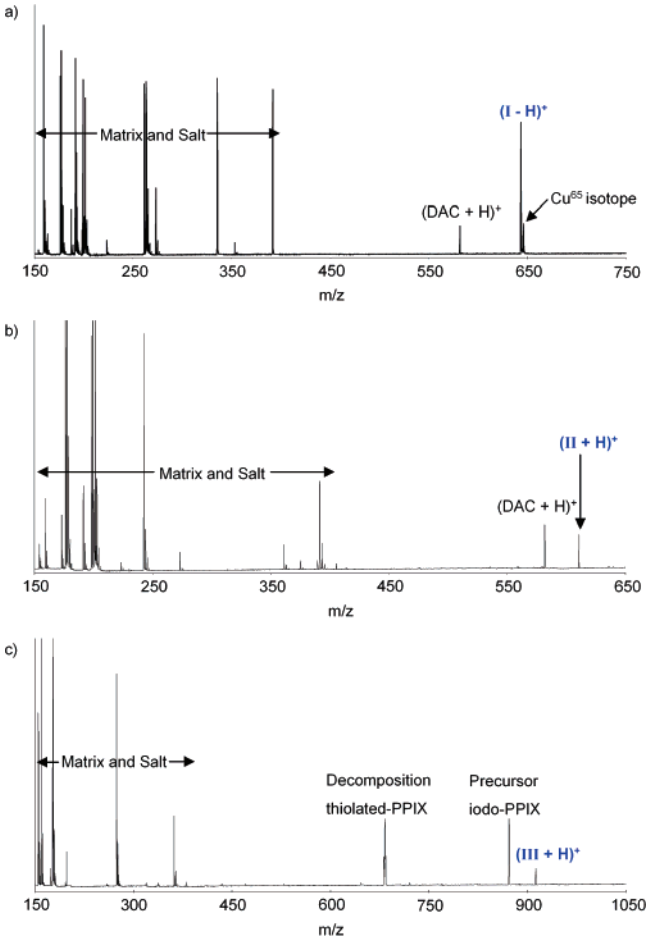

Figure 2. MALDI-TOF mass spectra of (a) **I**, (b) **II**, and (c) **III**. The cyclam deprotonates in **I** to form $(\mathbf{I} - H)^+$, while both **II** and **III** protonate to create $(\mathbf{II} + H)^+$ and $(\mathbf{III} + H)^+$ ions.

the porphyrin and iron salt as the only flexible part of **III** in constructing possible starting structures. In addition, structures in which the ester linkages were bound in the positions either syn or anti to the sulfurs were considered. Starting structures were first constructed using the program HyperChem.[39] The coordinates from each manually constructed structure were then used in subsequent DFT calculations in Jaguar[37] and Gaussian.[40] Calculations in Jaguar were performed using B3LYP/LACVP*,[34−36] and in all cases a final optimization was done using Gaussian, reading in the basis set and ECP used in Jaguar.

Several optimized structures were subsequently protonated at one of the two free nitrogens in the porphyrin ring and reoptimized to see the effect on the relative energies and cross sections. Although the cross sections did not significantly change for the protonated forms, the energies of the more compact, folded structures were somewhat lowered compared to those of the fully open structure (3−4 kcal/mol). Due to SCF convergence issues for some of the protonated structures, and because further optimization required several weeks of computer time for each structure, further calculations on the protonated species were not carried out. The ultimate goal of the calculations is to identify structures having cross sections consistent with the experimentally observed ion mobilities rather than to predict structures a priori.

Results and Discussion

Mass Spectra. MALDI-TOF mass spectra for **I**, **II**, and **III** are shown in Figure 2. Fragment peaks occur for all three systems; however, the peaks below *m*/*z* 400 are not from fragmentation but are due to the matrix and salt used in sample preparation. Two *m*/*z* peaks are observed in the mass spectrum for **I**. The smaller *m*/*z* peak corresponds to $(DAC + H)^+$, and the higher *m*/*z* peak corresponds to the deprotonated parent ion $(\mathbf{I} - H)^+$, where the cyclam is deprotonated. Two peaks are also seen in the mass spectrum of **II**, with the smaller *m*/*z* peak corresponding to $(DAC + H)^+$ and the higher *m*/*z* peak corresponding to the protonated parent ion $(\mathbf{II} + H)^+$. Three peaks are seen in the mass spectrum for **III**. The two smallest *m*/*z* peaks correspond to a light decomposition product (thiolated-PPIX) and a precursor (iodo-PPIX), while the highest *m*/*z* peak is for the protonated parent ion, $(\mathbf{III} + H)^+$. Each of the three ions of interest, $(\mathbf{I} - H)^+$, $(\mathbf{II} + H)^+$, and $(\mathbf{III} + H)^+$, were mass selected and gently injected into the drift cell so that their ATDs could be collected. A discussion of ion mobility results follows.

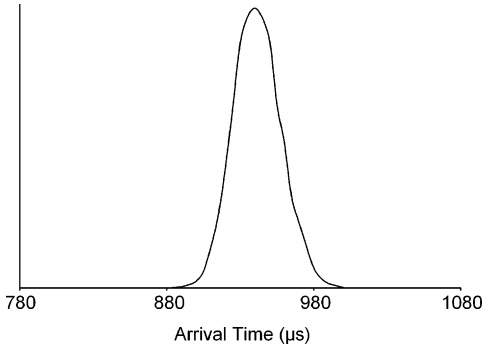

Figure 3. Arrival time distribution (ATD) for $(\mathbf{I} - H)^+$ at 80 K. Only one peak occurs in the ATD, indicating that only one conformer is present in the experiment.

$(\mathbf{I} - H)^+$. Only one peak, with a cross section of 161 Å^2, was observed in the 300 K ATD obtained for $(\mathbf{I} - H)^+$. A single, symmetric peak in an ATD signifies that either one family of conformers is present or multiple conformers are present that rapidly interconvert in the drift cell on the time scale of the experiment (∼1 ms). To slow most isomerization processes and separate multiple conformers,[41,42] the temperature of the drift cell was lowered to 80 K, and again a single-peak ATD was acquired (Figure 3). The width of the peak coincides with the width predicted from kinetic theory,[30] indicating that only a single conformer exists in the experiment.

The X-ray crystal structure of **I** (ORTEP)[14] is shown in Figure 4. Only one crystal structure was observed, where Cu^{II} sits inside the cyclam with one anthracenyl chromophore positioned above the cyclam and the other below. Since only one conformation was observed for **I** in the solid state and in the gas phase, theoretical modeling was performed to determine whether the gas-phase structure agrees with the solid-state structure.

Low-energy structures obtained from AMBER molecular mechanics/dynamics for $(DAC - H)^-$ with the anthracenyl arms in various arrangements were used as starting structures for DFT calculations. Cu^{II} was then added at a variety of prospective binding sites, and the geometry of each structure was optimized by DFT calculations in order to elucidate where Cu^{II} coordination occurs and how the corresponding theoretical cross section of each complex was affected by the coordination. The lowest

(39) *HyperChem*, Release 7.51; HyperCube, Inc.: Gainesville, FL, 2002.
(40) Frisch, M. J.; et al. *Gaussian 03*, Revision B.04; Gaussian, Inc.: Pittsburgh, PA, 2003.
(41) Gidden, J.; Wyttenbach, T.; Batka, J. J.; Weis, P.; Bowers, M. T.; Jackson, A. T.; Scrivens, J. H. *J. Am. Soc. Mass Spectrom.* **1999**, *10*, 883.
(42) Gidden, J.; Bowers, M. T. *Eur. Phys. J. D* **2002**, *20*, 409.

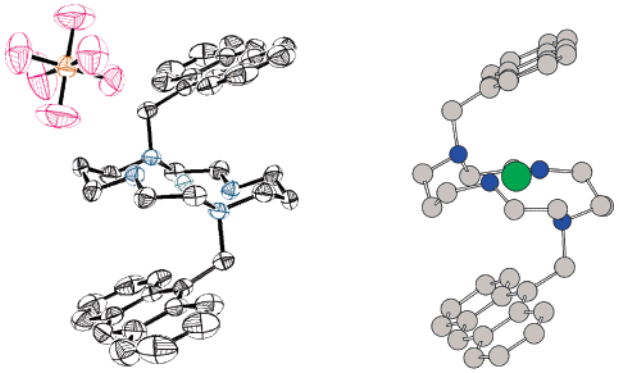

Figure 4. Crystal structure for **I**[14] and the lowest energy DFT structure for $(\mathbf{I} - H)^+$. The crystal and DFT structures are very similar. The crystal structure shown includes one of the PF_6^- anions. Carbon atoms are gray, nitrogens are blue, and Cu^{II} is green. All hydrogens are omitted for clarity.

Table 1. Experimental (300 K) and Theoretical Collision Cross Sections of $(\mathbf{I} - H)^+$, $(\mathbf{II} + H)^+$, and $(\mathbf{III} + H)^+$

ion	expt (Å²)[a]	theory (Å²)
$(\mathbf{I} - H)^+$	161	166[b]
$(\mathbf{II} + H)^+$	159, 173	161, 172[c]
$(\mathbf{III} + H)^+$	200, 210	see text

[a] 1% reproducibility error. [b] 3% standard deviation. [c] 2% standard deviation.

energy structure from the DFT calculations had a cross section of 166 ± 5 Å² and was the only conformation to agree with the experimental cross section (Table 1). In this structure, Cu^{II} sits inside the cyclam, with one anthracenyl chromophore positioned above the cyclam and the other below, as shown in Figure 4. The crystal structure of **I** agrees very well with the DFT structure for $(\mathbf{I} - H)^+$, which agrees well with the experimental cross section, suggesting that **I** has similar structures in the gas phase and in the solid state.

$(\mathbf{II} + H)^+$. The organic product of the reaction depicted in Scheme 1 was identified as **II**, where the cupric ion is ejected from the ligand.[14] A positive-ion ESI-MS analysis of the product from the reaction of **I** with $^{14}N^{16}O$ demonstrated that the cyclam itself was nitrosylated (*m/z* 610, corresponding to $(DAC\text{-}^{14}N^{16}O + H)^+$), and this was confirmed using doubly labeled $^{15}N^{18}O$ (*m/z* 613, corresponding to $(DAC\text{-}^{15}N^{18}O + H)^+$). An IR band at 1430 cm^{-1} in acetonitrile was also observed, consistent with the expected ν_{NO} of a nitrosoamine for the modified ligand.[43] However, further analysis with NMR led to questions about the structure of **II**. In the ^1H NMR spectrum of **II** in perdeuterio acetonitrile, the presence of two independent species corresponding to **II** in a ~1:1 ratio was observed (20 signals in the aliphatic region). The two sets consisted of four protons at 4.16, 3.88, 3.47, and 3.39 ppm, which appeared at values lower than expected for normal cyclam ring protons but were consistent with the chemical shifts for α-protons of an aliphatic nitrosoamine.[44,45] However, the structures could not be unambiguously determined from the chemical shifts.

In the ion mobility measurements of $(\mathbf{II} + H)^+$, two resolvable features with cross sections of 159 and 173 Å² were

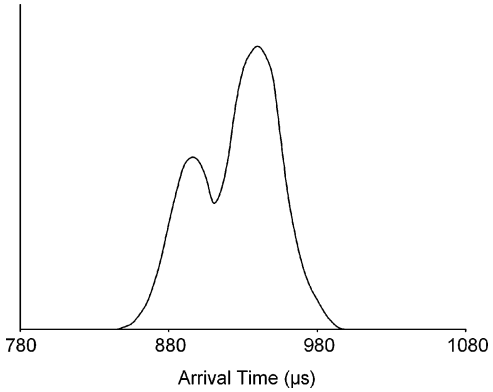

Figure 5. ATD for $(\mathbf{II} + H)^+$ obtained at 80 K. Two peaks occur in the ATD and indicate that two conformers of $(\mathbf{II} + H)^+$ are present in the experiment.

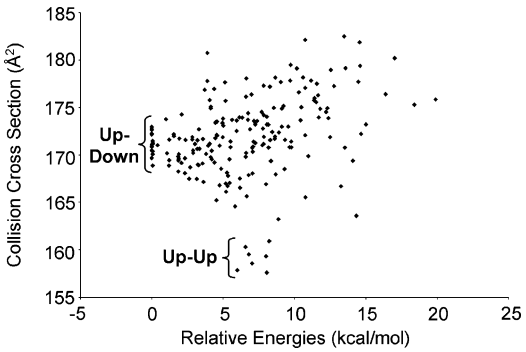

Figure 6. Scatter plot of cross section vs energy for $(\mathbf{II} + H)^+$. Each point represents one theoretical structure. Two different families of conformers are predicted for $(\mathbf{II} + H)^+$, depending on the position of the anthracenyl groups. The lower energy family has one anthracenyl group above the cyclam and the other below (Up−Down). The higher energy family has anthracenyl groups on the same side of the cyclam (Up−Up).

apparent in the ATD (Figure 5). Two peaks indicate that two distinct, non-interconverting conformers exist (as suggested by the ^1H NMR results). The temperature of the drift cell was decreased from 300 to 80 K to slow any possible isomerization between conformers and to increase the resolution of the ATD.[28] No new peaks were observed at 80 K, but the resolution did increase. Figure 5 illustrates the high-resolution 80 K ATD, where the two peaks occur in a ratio of 2:3, indicating that 40% of $(\mathbf{II} + H)^+$ exists as a smaller conformer, while 60% exists as a larger conformer.

Theoretical structures for $(\mathbf{II} + H)^+$ were generated using the AMBER theoretical methods described in the Experimental Section, since no transition metals are present in **II**. A plot of cross section versus energy from the theoretical calculations is shown in Figure 6. Two distinct families of structures were observed in the scatter plot, depending on the position of the anthracenyl chromophores. Each family of structures is represented in Figure 7. The lowest energy structures with the largest cross section (172 ± 3 Å²) occur when one anthracenyl is positioned above the cyclam while the other anthracenyl is below. This indicates that some of the conformers of $(\mathbf{II} + H)^+$ have anthracenyl groups in an Up−Down configuration, similar to the structure observed for $(\mathbf{I} - H)^+$. The second family of conformers, ~6 kcal/mol higher in energy according to AMBER, have an average cross section of 161 ± 3 Å². In this

(43) Lee, J.; Chen, L.; West, A. H.; Richter-Addo, G. B. *Chem. Rev.* **2002**, *102*, 1019.
(44) Karabatsos, G. J.; Taller, R. A. *J. Am. Chem. Soc.* **1964**, *86*, 4373.
(45) Cooney, J. D.; Brownstein, S. K.; ApSimon, J. W. *Can. J. Chem.* **1974**, *52*, 3028.

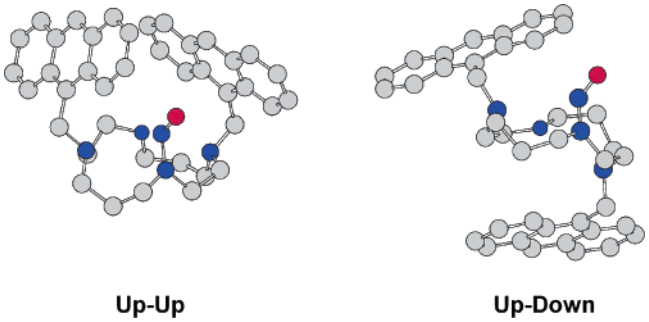

Figure 7. Examples of the two families predicted for (**II** + H)$^+$. The Up−Down family is the lower energy family, with one anthracenyl above the cyclam and one below. The Up−Up family has both anthracenyl groups on the same side of the cyclam. Carbon atoms are gray, nitrogens are blue, oxygen is red, and all hydrogens are omitted for clarity.

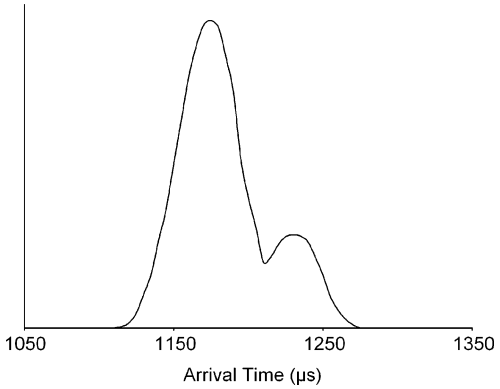

Figure 8. ATD for (**III** + H)$^+$ obtained at 80 K. Two peaks occur in the ATD, signifying that two conformers of (**III** + H)$^+$ are present in the experiment.

family of structures, both anthracenyl groups are positioned above the cyclam in an Up−Up conformation.

The average cross section of the lowest 5 kcal/mol structures in each family of conformers was used for comparison with the experimental cross sections obtained from the ATD. The theoretical cross section for the family of conformers with both anthracenyl groups positioned on the same side of the cyclam agrees very well with the cross section obtained for the shortest time peak in the ATD, while the cross section for the family with one anthracenyl group above the cyclam and one below agrees with the cross section obtained for the longest time peak (Table 1). From the relative intensities of each peak, it appears that 40% of (**II** + H)$^+$ structures have both anthracenyl groups on the same side of the cyclam, while 60% have one anthracenyl group above the cyclam and one below.

(III + H)$^+$. Compound **III** was studied in order to evaluate the hypothesis that PPIX-RSE may exist as two geometric isomers in solution. This hypothesis was formulated on the basis of two photophysical features: the bimodal fluorescent decay giving lifetimes of 0.22 and 10.4 ns, both shorter than that of free PPIX (13.2 ns), and the residual emission in the steady-state luminescence experiments. The pre-exponential factors indicate that the shorter lifetime species represents about 80% of the excited states. It was proposed that this behavior was due to the presence of two conformers (or families of conformers), one being more compact than the other with the iron/sulfur/nitrosyl cluster positioned closer to the PPIX chromophore. The IM-MS experiments appear consistent with this hypothesis, since two resolvable features with cross sections of 200 and 210 Å^2 are apparent in the ATD for (**III** + H)$^+$ (Figure 8), and the more intense peak has the smaller cross section (i.e., is more compact). When the temperature of the drift cell was decreased from 300 to 80 K, the resolution increased, but no new peaks were observed. The injection energy was increased from 30 to 150 eV with no change in the 80 K ATD. At 300 K, a modest (∼10%) increase in the minor component at longer times was observed at the highest injection energies, indicating that this conformer may be slightly more stable than the more tightly folded one in solvent-free conditions. No new peaks were observed. Figure 8 illustrates the higher resolution 80 K ATD, which displays two peaks in a ratio of 3:1, indicating that 75% of (**III** + H)$^+$ exists as the smaller conformer, while 25% exists as a larger conformer.

The computational studies of **III** give a more complex picture. Nine different (neutral) structures for **III** were successfully optimized in the DFT calculations. The structures ranged from ones that were folded, such that the iron salt was close to the porphyrin ring, to a completely unfolded structure, in which the iron salt is at a maximum distance from the porphyrin. The lowest energy structure predicted by DFT was the completely unfolded one. However, the cross section for this structure was much larger (241 Å^2) than the experimentally determined cross sections, and clearly it does not correspond to the observed ions. Comparison of experimental and theoretical cross sections suggests the dominance of folded structures, a result that is consistent with the photophysical data in solution. As noted in Figure 9, several of these higher energy folded structures show cross sections close to those determined experimentally.

As noted in the Experimental Section, several structures were reoptimized as protonated species, which lowered the energies of the folded structure by 3−4 kcal/mol. This still gives a lower energy for the unfolded structure, though only by 2 kcal/mol compared to the lowest energy folded structure. The lack of dispersion energy in the B3LYP functional could account for an addition lowering in energy of the folded structures, but higher level calculations were deemed too computationally expensive to investigate the effects of dispersion. However, the main point of the calculations is to identify structures consistent with the experimentally measured cross sections rather than to predict their conformations a priori. The fact remains that, experimentally, two distinct sizes of (**III** + H)$^+$ were observed, and they clearly are not consistent with the unfolded form.

As discussed in the Introduction, initial excitation of the porphyrin chromophore of PPIX-RSE is apparently followed by energy transfer from the PPIX excited state to the $Fe_2S_2(NO)_4$ unit, followed by NO release from the cluster. If it is assumed that the decrease in the fluorescent lifetimes seen for the two conformers of PPIX-RSE (10.4 and 0.22 ns) relative to that for PPIX itself (13.2 ns)[12b] is entirely due to this energy-transfer process, then the respective intramolecular energy-transfer rate constants (k_{en}) are calculated to be 2.0×10^7 and 4.5×10^9 s^{-1}. For energy transfer via the Förster mechanism, the rate should demonstrate an r_i^{-6} dependence, where r_i is the distance between donor and acceptor for a specific system.[46] On this basis, the ratio of the energy-transfer rate constants for conformers 1 and 2, $k_{en}(1)/k_{en}(2)$, should equal $(r_2/r_1)^6$ if one assumes that the only parameter altered between the two different PPIX-

(46) Förster, Th. In *Modern Quantum Chemistry*; Sinanoglu, O., Ed.; Academic Press: New York, 1973.

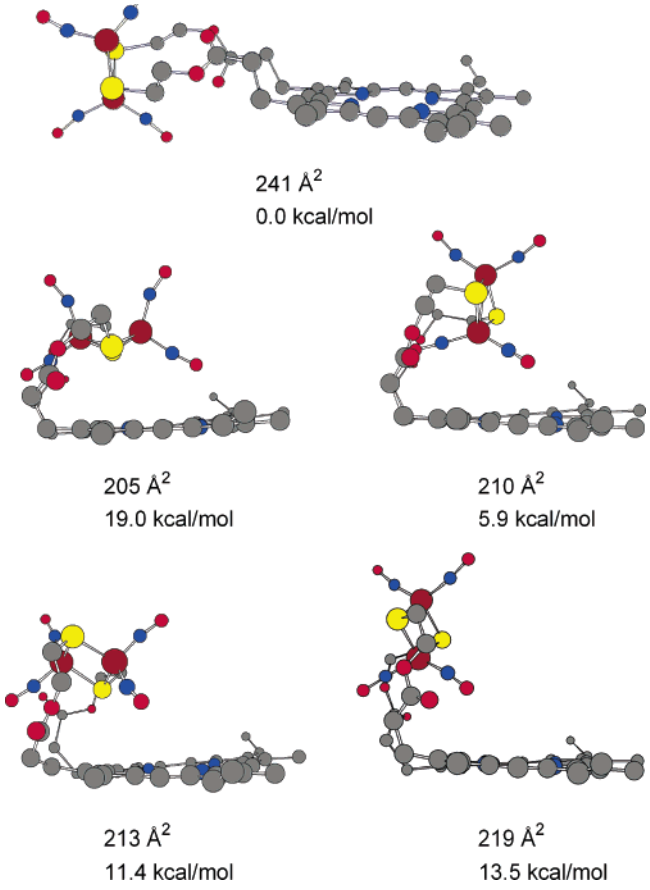

Figure 9. Representative DFT optimized structures of **III**. The four folded structures are within the range of the two experimental cross sections, but the open structure, although predicted to be the lowest energy structure, would have a much larger cross section.

RSE geometric isomers is the distance between the iron−sulfur core and the porphyrin ring. An obvious problem in evaluating such a relationship is determining what distances appropriately represent values of r_i. A rough approximation, based on the distance between the center of the porphyrin ring and the midpoint of the two irons in the $Fe_2S_2(NO)_4$ cluster gives, $r_1 = 4.6$ Å and $r_2 = 7.3$ Å for the folded structures with cross sections of 205 and 219 Å^2 (the smallest and largest DFT structures matching the experimental cross sections). These distances give a value of 16 for $(r_2/r_1)^6$, consistent with the view that the energy-transfer rates should be considerably different for the two conformers; however, it is notable that the experimental $k_{en}(1)/k_{en}(2)$ ratio, at 225, is more than an order of magnitude larger than the estimate. One likely contribution to this difference is the uncertainty regarding how to estimate r_1 and r_2. Another possible source of the underestimated $k_{en}(1)/k_{en}(2)$ could be that the Förster mechanism for energy transfer is also influenced by the orientation of the transition dipoles of the chromophores relative to each other. In the estimate above, it was assumed that this was constant for the different conformers, but that assumption is likely to be flawed. On the other hand, if one examines the $(r_2/r_1)^6$ ratio for the minimized, fully unfolded structure ($r_2 \approx 11.7$ Å) versus the most compact of the folded structures, the value is about 270, somewhat larger but closer in magnitude to the experimental $k_{en}(1)/k_{en}(2)$ ratio. However, if this species were present in the sample studied by IM-MS, it should have been observed and not have isomerized to a more compact, higher energy structure during analysis. Hence, the difficulty in accurately estimating the Förster parameters from the structures that correlate with experiment is the most likely reason for the discrepancy.

Summary

Mass spectrometry, ion mobility, and theoretical modeling results presented in this paper provide several important insights into the conformations of chromophore-bound complexes. The primary observations are given below.

(1) The crystal structure for **I** and the lowest energy DFT structure that agrees with the experimental cross section for $(\mathbf{I} - H)^+$ are very similar, indicating that **I** has a similar structure in the solid state and in the gas phase.

(2) Before reductive nitrosylation takes place, only one conformation is seen for **I**, where one anthracenyl group is above the cyclam while the other is below the cyclam. However, IM-MS indicates that the reductive nitrosylation product **II** has two conformers, in which the anthracenyl groups are on opposite sides of the cyclam, similar to **I** (Up−Down configuration), or on the same side of the cyclam (Up−Up configuration). These results are consistent with solution data where two products are suggested but no structures obtained.

(3) Ion mobility experiments demonstrate the presence of two structures for $(\mathbf{III} + H)^+$, the more compact one being the more prevalent, which is in agreement with a dual lifetime for fluorescence decay in solution. Computational studies indicate that these are both partially folded structures, with the iron cluster folded over the protoporphyrin ring. The relative population of these conformers (or families of conformers), determined from ion mobility experiment, is in agreement with estimates of solution populations based on pre-exponential factors. However, a simple analysis using the Förster mechanism for these two structures was an order of magnitude smaller than the ratio of the observed rates.

(4) IM-MS appears to be a valuable new tool in structural elucidation of supramolecular complexes of the type described in this paper.

Acknowledgment. These studies were supported by grants from the National Science Foundation (CHE-0352650 to P.C.F. and CHE-0503728 to M.T.B.).

Supporting Information Available: Full citations for refs 31 and 40. This material is available free of charge via the Internet at http://pubs.acs.org.

JA0553699